Electronic Supplementary Material (ESI) for Chemical Communications.
This journal is © The Royal Society of Chemistry 2018

Supplementary Information for:

A self-assembled dual-phase composite as precursor of high-performance anode for Intermediate temperature solid oxide fuel cells

Yefeng Song, Yi-Mei Yin, Linsen Li, Zonghai Chen, Zi-Feng Ma**

Experimental Section

Sample preparation

$LS_{0.6}FCN$ precursor was synthesized using a solid-state reaction method. The stoichiometric amounts of La_2O_3, $SrCO_3$, Fe_2O_3, Cu_2O and Nb_2O_5 powders were mixed by ball milling for 24 h in a planetary ball miller, followed by uniaxially pressing the mixture at a pressure of 4 MPa into pellets. The pellets were calcined in air at 1000 °C for 10 h, subsequently grounded to obtain $LS_{0.6}FCN$ final powders.

Single cells with configuration of $LS_{0.6}FCN|SDC|ScSZ(200\ \mu m)|SDC|LS_{0.6}FCN$ were fabricated based on commercial ScSZ electrolyte pelletes purchased from SOFCMAN Company (Ningbo, China). The SDC ink was screen-printed onto both sides of the electrolyte and sintered at 1250 °C for 2 h to form a protection interlayer with the thickness of ~ 10 μm. Then the $LS_{0.6}FCN$ ink was screen-printed on the surface of the SDC interlayer and sintered at 900 °C for 2 h. The thickness and active area of the electrodes are ~30 μm and ~ 0.28 cm^2, respectively.

Sample Characterizations

The crystal structure of the powders before/after reduction are characterized by XRD measurements performed on an X-ray diffractometer (Rigaku D/max-2200/PC) with a Cu Ka radiation, λ = 0.15415 nm. The XRD patterns in the 2 theta range of 10-100° are refined by

using the Rietveld method of the FullProf_Suite program. The final agreement R-factors, the detailed Rietveld refinement parameters and crystal structure data of $LS_{0.6}FCN$ and R-$LS_{0.6}FCN$ are given in Table S1, Table S2 and Table S3.

The microstructures of the cross-section of porous $LS_{0.6}FCN$ pellets (pressed at 4 MPa and sintered at 900 °C for 10 h) before/after reduction were examined using SEM (Nova NanoSEM 450, FEI Company, USA) and HRTEM (JEM-2100, JEOL Ltd, Japan).

The I-V(P) curves of single cells were tested by four-probe configuration. The anode side is fed by fuels at the flow rate of 60 mL min^{-1}, while the cathode is exposed to static air as oxidant. The cell was heated to 800 °C and held for 2 h in fuels to ensure a stable output. EIS of the cells were collected via AC impedance method using electrochemical workstation (Autolab PGSTAT 302 N, USA) in temperature range of 600-800 °C. An AC signal with 10 mV amplitude and a frequency range from 10^{-2} Hz to 10^{6} Hz was applied as stimuli. The cells were stabilized at each testing temperature for 15 min before the EIS spectra were collected.

Supplementary Figures, tables and captions

Table S1(a) and (b) Details of Retvield Refinement Results of $LS_{0.6}FCN$ and R- $LS_{0.6}FCN$, respectively.

(a) $LS_{0.6}FCN$				
Phase No.	$SrLaFeO_4$-type		$Sr_{0.4}La_{0.6}FeO_3$-type	
Space Group	I 4/m mm		R -3 c	
Cell parameters	a(Å)	3.86674(118)	a(Å)	5.50040(52)
	b(Å)	3.86674(118)	b(Å)	5.50040(52)
	c(Å)	12.78770(544)	c(Å)	13.54159(198)
	α(°)	90	α(°)	90
	β(°)	90	β(°)	90
	γ(°)	90	γ(°)	120
	Volume($Å^3$)	191.192(116)	Volume($Å^3$)	354.809(70)
Fract(%)	16.75(0.77)		83.25(0.96)	
R-factors	Rwp	11.2%		
	Rp	8.77%		
	Rexp	9.64%		
	χ^2	1.34		

(b) R-$LS_{0.6}FCN$				
Phase No.	$SrLaFeO_4$-type	$LaFeO_3$-type	Fe^0	Cu^0

Space Group		I 4/m mm	P b n m	I m -3 m	F m -3 m
Cell	a(Å)	3.88427(11)	5.57475(57)	2.86447(29)	3.61784(56)
parameters	b(Å)	3.88427(11)	5.57122(41)	2.86447(29)	3.61784(56)
	c(Å)	12.71767(66)	7.84557(76)	2.86447(29)	3.61784(56)
	α(°)	90.0	90.0	90.0	90.0
	β(°)	90.0	90.0	90.0	90.0
	γ(°)	90.0	90.0	90.0	90.0
	Volume($Å^3$)	191.871(13)	243.669(34)	23.503(4)	47.351(13)
Fract(%)		62.83(57)	27.44(36)	8.30(44)	1.43(15)
R-factors	Rwp		12.1%		
	Rp		9.25%		
	Rexp		10.00%		
	$\chi 2$		1.47		

Table S2. Atomic Coordinates and atom site occupancy for $LS_{0.6}FCN$.

$SrLaFeO_4$-type phase (SLF214)					
atom	Multi	x	y	z	Occ.
Sr1	4	0	0	0.35512(221)	0.5
La1	4	0	0	0.35512(221)	0.5
Fe1	2	0	0	0	0.801(3)
Cu1	2	0	0	0	0.141(2)
Nb1	2	0	0	0	0.054(3)
O1	4	0	0.5	0	1.0
O2	4	0	0	0.16634(687)	1.0
$Sr_{0.4}La_{0.6}FeO_3$-type phase (SLF113)					
La1	6	0	0	0.25	0.713(2)
Sr1	6	0	0	0.25	0.287(2)
Fe1	6	0	0	0	0.832(3)
Cu1	6	0	0	0	0.182(4)
Nb1	6	0	0	0	0.007(5)
O1	18	0.19449(426)	1/3	1/12	0.993(5)

Table S3. Atomic Coordinates and atom site occupancy for R-$LS_{0.6}FCN$.

$SrLaFeO_4$-type phase (SLF214)					
atom	Multi	x	y	z	Occ.
Sr1	4	0	0	0.35742(21)	0.5
La1	4	0	0	0.35742(21)	0.5
Fe1	2	0	0	0	1.0
O1	4	0	0.5	0	1.0
O2	4	0	0	0.16865(138)	1.0
$LaFeO_3$-type phase (LFO113)					
La1	4	0.98542(162)	0.01653(163)	0.25	1.0
Fe1	4	0	0.5	0	1.11(5)
O1	8	0.71910(231)	0.30281(212)	0.02910(311)	1.06(7)
O2	4	0.08996(175)	0.39247(346)	0.25	1.36(13)
Fe^0 phase					
Fe1	2	0	0	0	1.0
Cu^0 phase					
Cu1	4	0	0	0	1.0

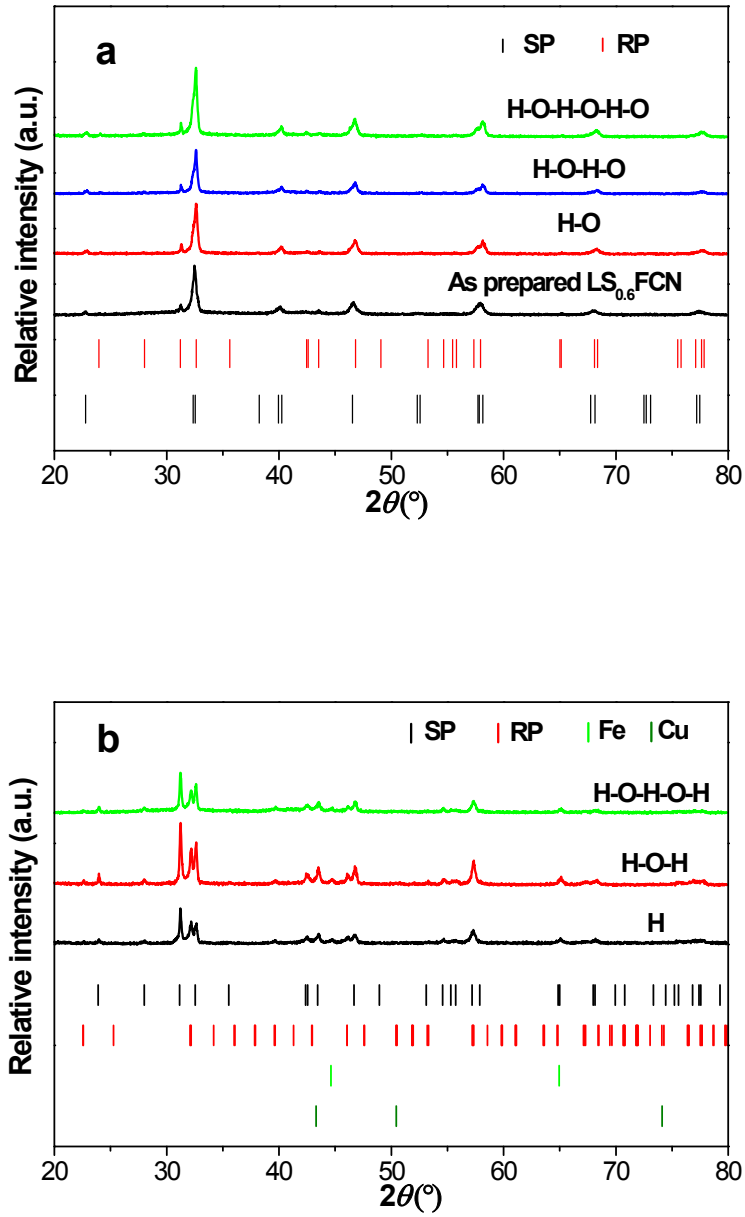

Figure S1 XRD patterns of the as-prepared $LS_{0.6}FCN$ powders in 3 redox cycles at 800 °C (a) in air and (b) in humified H_2 (3%), respectively, for 10 h.

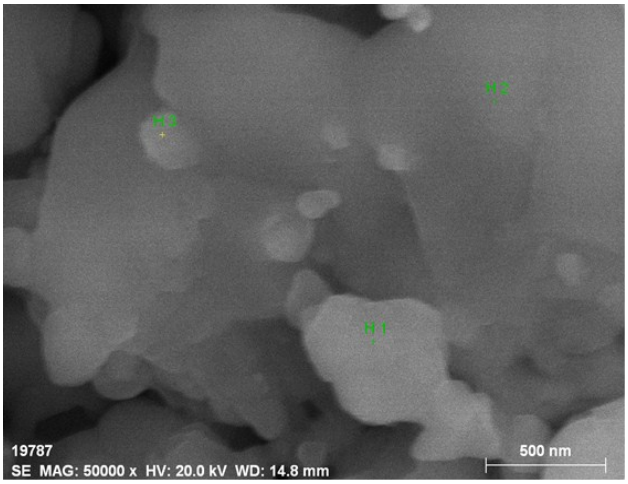
H3
H2
H1
19787
SE MAG: 50000 x HV: 20.0 kV WD: 14.8 mm
500 nm

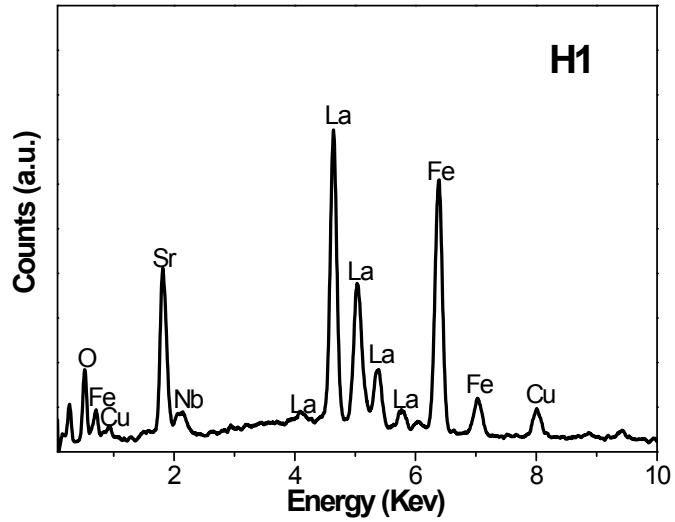
H1
Counts (a.u.)
Energy (Kev)
O
Fe
Cu
Sr
Nb
La
La
La
La
Fe
Fe
Cu
2
4
6
8
10

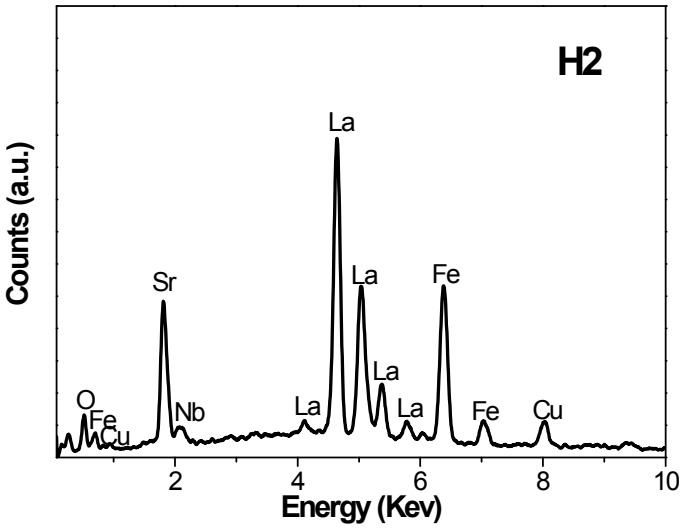
H2
Counts (a.u.)
Energy (Kev)
O
Fe
Cu
Sr
Nb
La
La
La
La
Fe
Fe
Cu
2
4
6
8
10

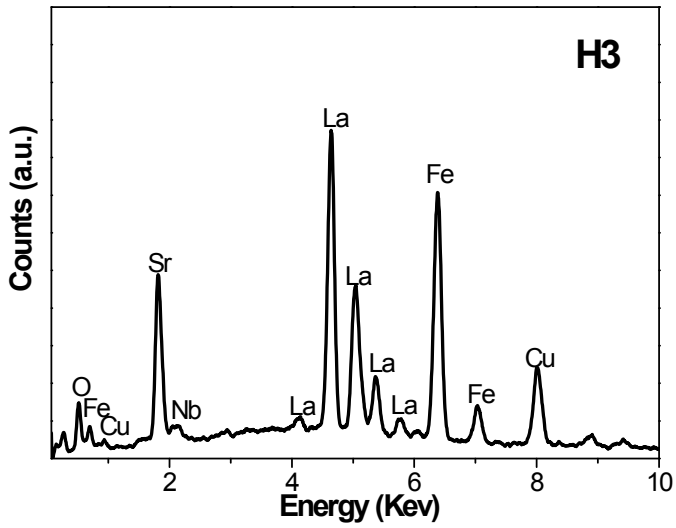

Figure S2 EDS spectra of regions (H1, H2, H3) on the $LS_{0.6}FCN$ pellet after reduction in humified H_2 (3% H_2O) at 800 °C for 20 h.

Table S4 The element distribution of the three regions in the $LS_{0.6}FCN$ pellet after reduction in humified H_2 at 800 °C for 20 h identified by EDS of SEM

Atomic con.	La	Sr	Fe	Cu	Nb
H1	0.52	0.58	**0.90**	0.13	0.09
H2	0.64	0.46	0.62	0.11	0.03
H3	0.58	0.52	**0.82**	**0.35**	0.04

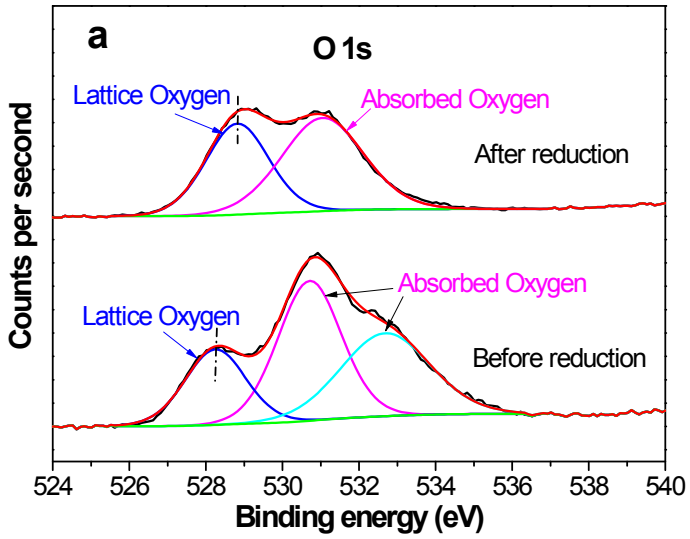
a
O 1s
Lattice Oxygen
Absorbed Oxygen
After reduction
Absorbed Oxygen
Lattice Oxygen
Before reduction
Counts per second
524 526 528 530 532 534 536 538 540
Binding energy (eV)

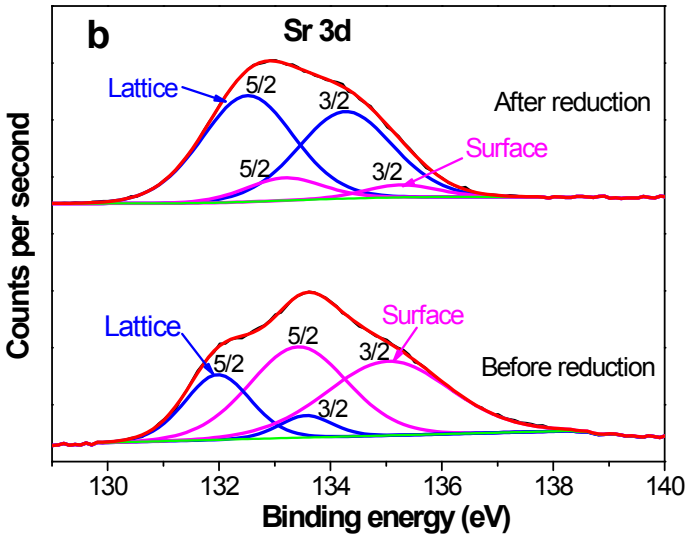
b
Sr 3d
Lattice
5/2
3/2
After reduction
Surface
5/2
3/2
Lattice
Surface
5/2
5/2
3/2
3/2
Before reduction
Counts per second
130 132 134 136 138 140
Binding energy (eV)

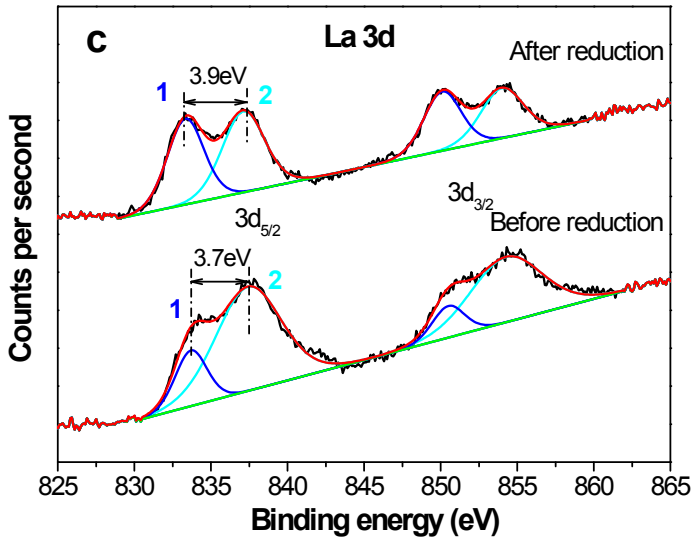
c
La 3d
After reduction
3.9eV
1
2
3d5/2
3d3/2
Before reduction
3.7eV
2
1
Counts per second
825 830 835 840 845 850 855 860 865
Binding energy (eV)

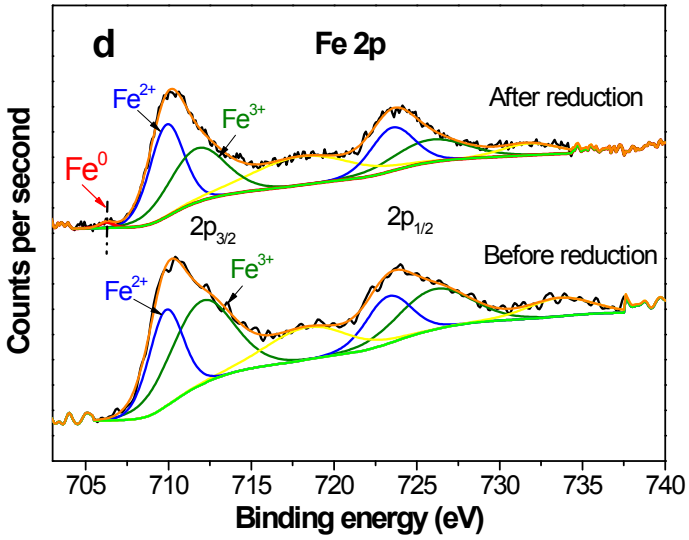
d
Fe 2p
Fe2+
Fe3+
Fe0
After reduction
2p3/2
2p1/2
Before reduction
Fe2+
Fe3+
Counts per second
705
710
715
720
725
730
735
740
Binding energy (eV)

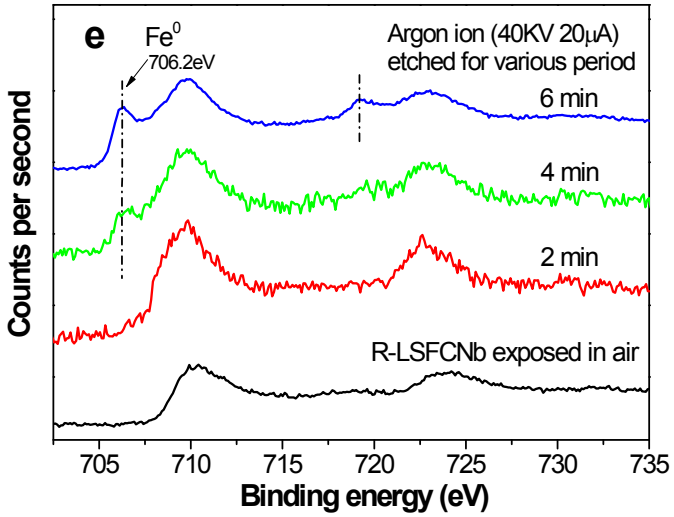
e
Fe0
706.2eV
Argon ion (40KV 20μA)
etched for various period
6 min
4 min
2 min
R-LSFCNb exposed in air
Counts per second
705
710
715
720
725
730
735
Binding energy (eV)

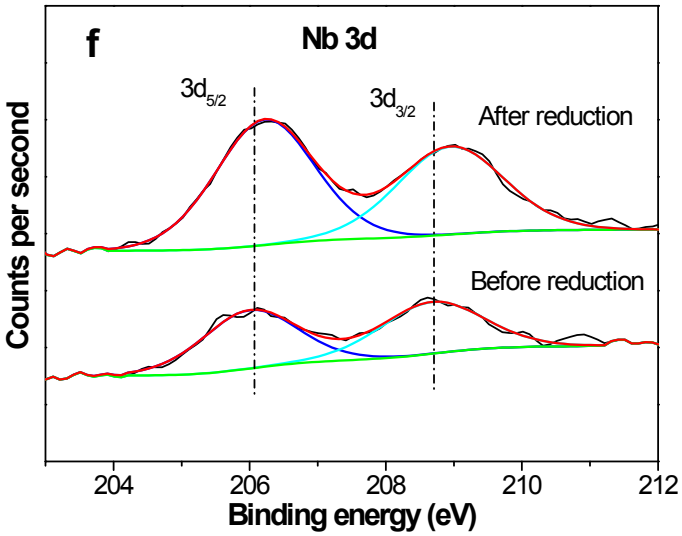
f
Nb 3d
3d5/2
3d3/2
After reduction
Before reduction
Counts per second
204
206
208
210
212
Binding energy (eV)

Figure S3 XPS spectra of the $LS_{0.6}FCN$ powders before and after reduction for (a) O1s, the relative intensity of lattice oxygen increases after reduction, suggesting that more RP phase formed at the surface of the reduced sample; (b) Sr 3d, the XPS spectra of Sr-3d demonstrate that the lattice Sr component (132-132.7eV) becomes much greater relative to the surface Sr component (133.4-134) after reduction, which is an indication of formation of RP phase at the surface of SP substrate on heating at low oxygen partial pressure as proved by a previous work.[S1] (c) La 3d, the binding energy difference of the splited La 3d5/2 peaks slightly increases, and the relative intensity of the peak at a higher binding energy position obviously decreases after reduction, which are indications of the transformation of La-CO_3 bond in air to La-OH bond in wet H_2 (https://xpssimplified.com/elements/lanthanum.php). (d) Fe 2p, a weak signal of Fe^0 can be observed at 706.2eV for the reduced sample possibly due to partial oxidation of metallic Fe at top surface in the transfer of the sample from lab oven to XPS instrument, and the relative intensity of Fe^{2+} signal increases after reduction; (e) After 4-min Ar+ ion etch on the reduced sample, a new peak clearly appeared at 706.2eV on the shoulder of the Fe ($2p_{3/2}$) region, which corresponds to the presence of metallic Fe. (f) Nb 3d, the intensity of Nb3d 5/2 increases after reduction suggests that the Nb element may be enriched at surface in the environment with more lattice oxygen.

$$A_{y+x}B_{y+\frac{x}{2}}O_3 + \frac{3-3y-2x}{2}O_2 \xrightarrow{In\ air} yABO_3 + \frac{x}{2}A_2BO_4 \quad (1)$$

$$\downarrow$$

$$2ABO_3 + 2H_2 \xrightarrow{In\ wet\ H_2} A_2BO_4 + B + 2H_2O \quad (2)$$

Figure S4 A proposed self-assemble mechanisms in the form of chemical reactions in air and in wet H_2

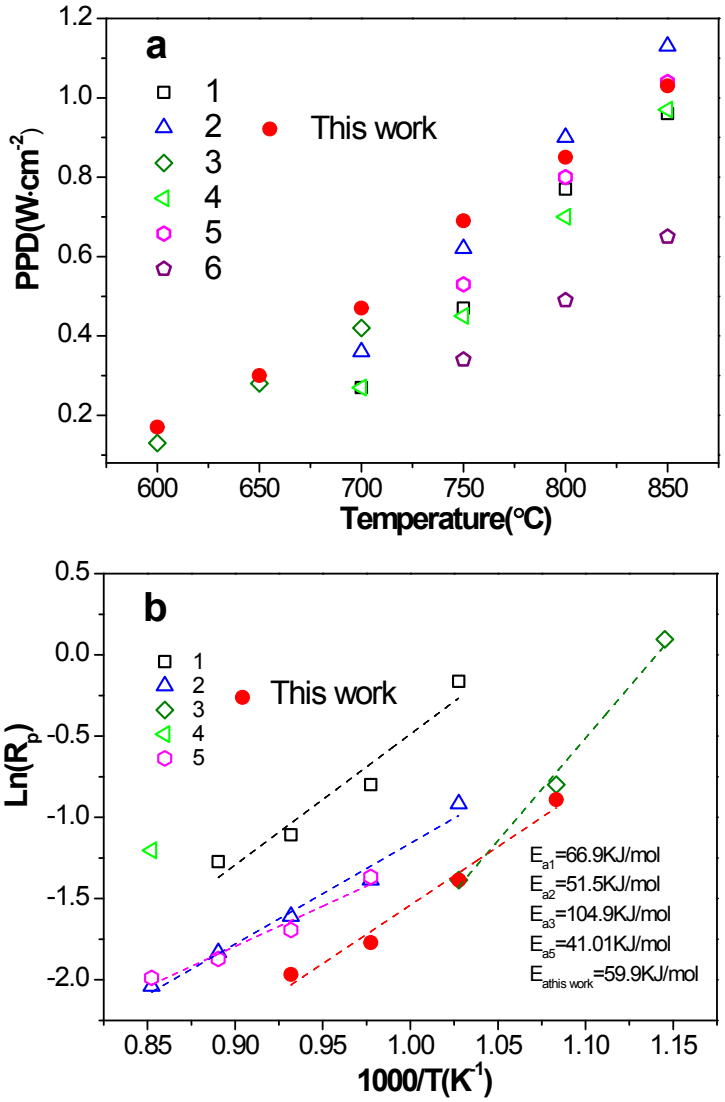

Figure S5 Arrhenius plots of peak power density (PPD) and polarization resistance (R_p) of ScSZ electrolyte supported full cell with R-$LS_{0.6}FCN$ anode compared with the cells with oxide composite anodes prepared from single perovskite precursors fed with H_2 fuel:

(1) $Pr_{0.8}Sr_{1.2}(Co,Fe)_{0.8}Nb_{0.2}O_{4+\delta}$-CFA|LSGM(300μm)|$Pr_{0.4}Sr_{0.6}Co_{0.2}Fe_{0.7}Nb_{0.1}O_{3-\delta}$;[S2]

(2) $Pr_{0.8}Sr_{1.2}(Co,Fe)_{0.8}Nb_{0.2}O_{4+\delta}$-CFA|LSGM(300μm)|$Ba_{0.9}Co_{0.7}Fe_{0.2}Nb_{0.1}O_{3-\delta}$; [S2]

(3) $SrFe_{0.8}Cu_{0.1}Nb_{0.1}O_{3-\delta}$|YSZ(100μm)|$La_{0.8}Sr_{0.2}FeO_{3-\delta}$; [S3]

(4)$La_{0.43}Ca_{0.37}Ni_{0.06}Ti_{0.94}O_{3-\delta}$|$Zr_{0.89}Sc_{0.1}Ce_{0.01}O_{2-\delta}$(ScSZ:140μm)|$Zr_{0.89}Sc_{0.1}Ce_{0.01}O_{2-\delta}$–$(La_{0.8}Sr_{0.2})_{0.95}MnO_{3-\delta}$;[S4]

(5) $Sr_2FeMo_{2/3}Mg_{1/3}O_{6-\delta}$|LDC|LSGM(300μm)|$La_{0.58}Sr_{0.4}Co_{0.2}Fe_{0.8}O_{3-\delta}$;[S5]

(6) $La_{0.4}Sr_{0.6}Co_{0.2}Fe_{0.7}Nb_{0.1}O_{3-\delta}$|LSGM(300μm)|$La_{0.4}Sr_{0.6}Co_{0.2}Fe_{0.7}Nb_{0.1}O_{3-\delta}$;[S6]

This work: $LS_{0.6}FCN|SDC|ScSZ(200\mu m)|SDC|LS_{0.6}FCN$

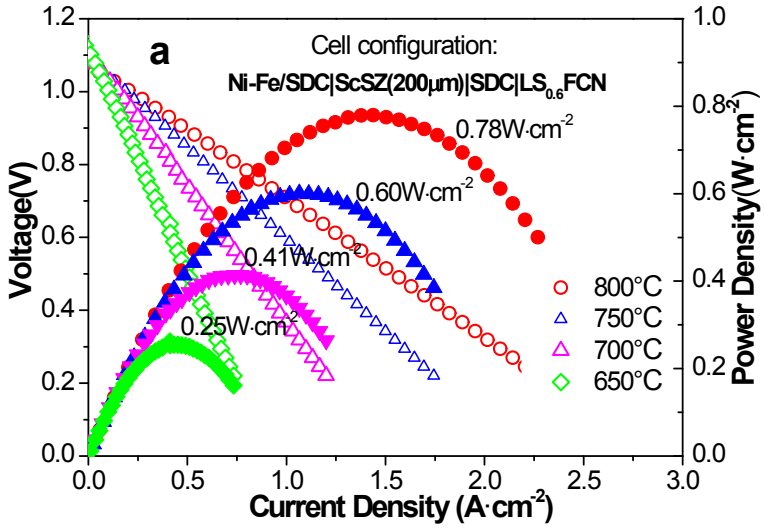

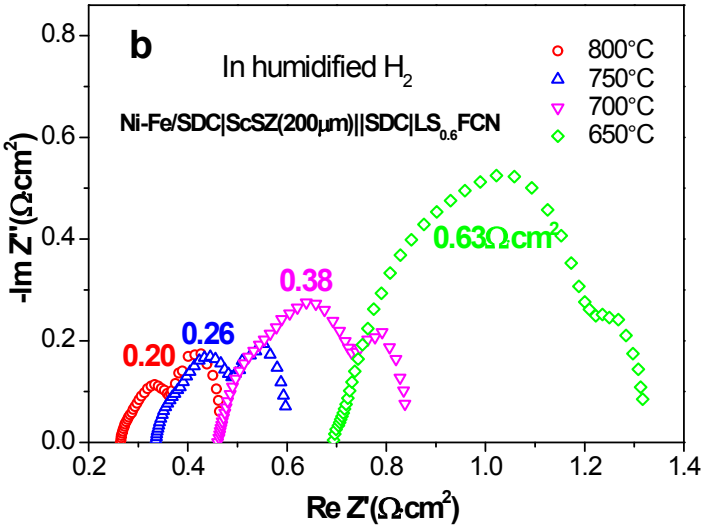

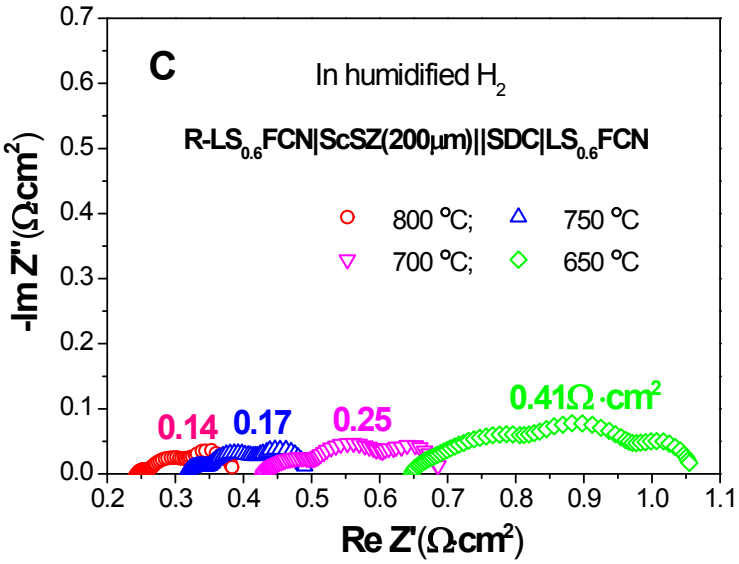

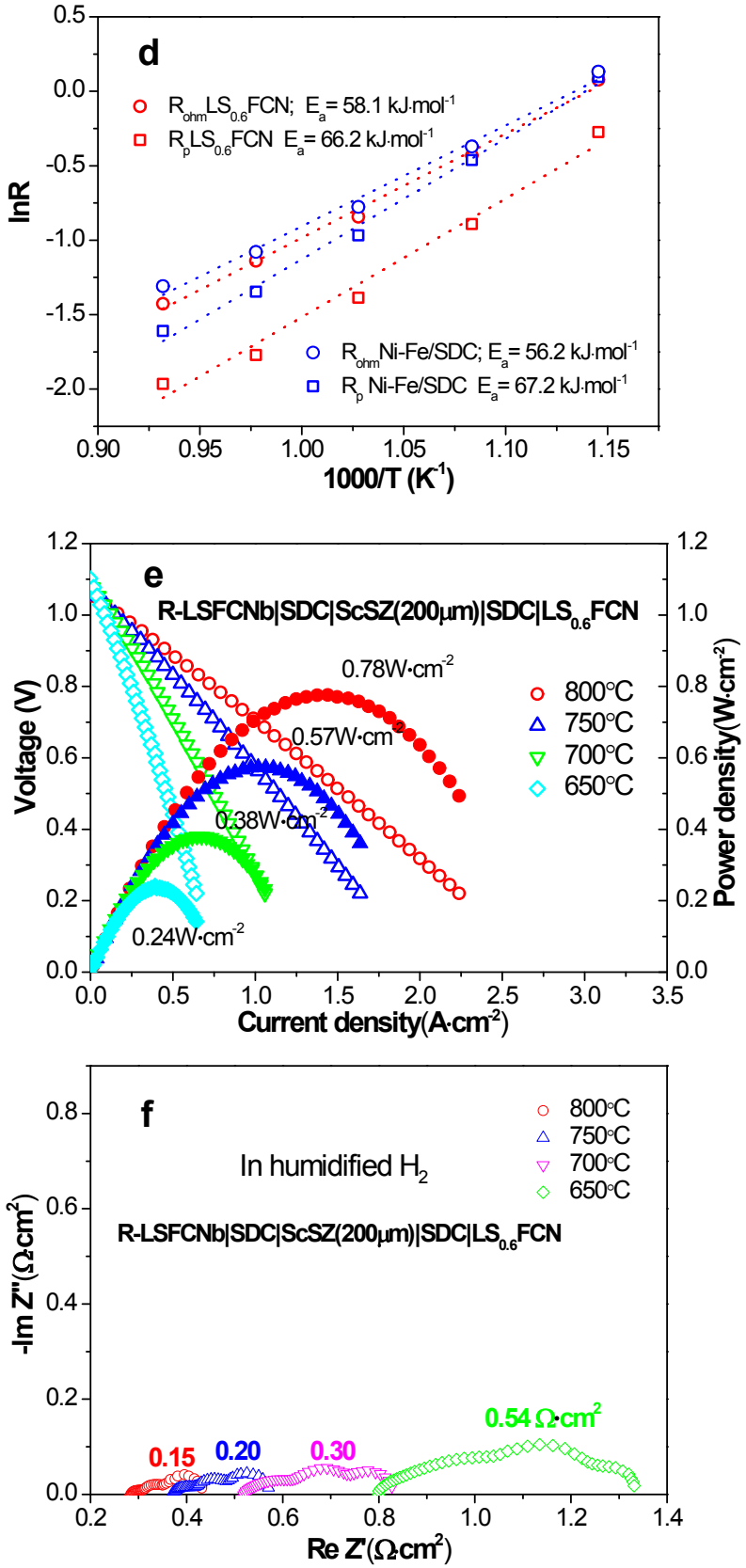

Figure S6 (a) I-V(P) curves of the cells with Ni-Fe/SDC cermet anode measured at various temperatures with static air as oxidant and humidified H_2 (3% H_2O) as fuel; (b) Corresponding EIS of the cell with Ni-Fe/SDC cermet anode at 650-800 °C; (c) EIS of the cell with R-

$LS_{0.6}FCN$ anode at 650-800 °C; (d) Arrhenius plots of R_p and R_{ohm} of the cells with R-$LS_{0.6}FCN$ and Ni-Fe/SDC cermet anodes, respectively. (e) I-V(P) curves of the cells with the R-LSFCNb anode in humidified H_2 at 650-800 °C; (f) Corresponding EIS of the R-LSFCNb cell at 650-800 °C.

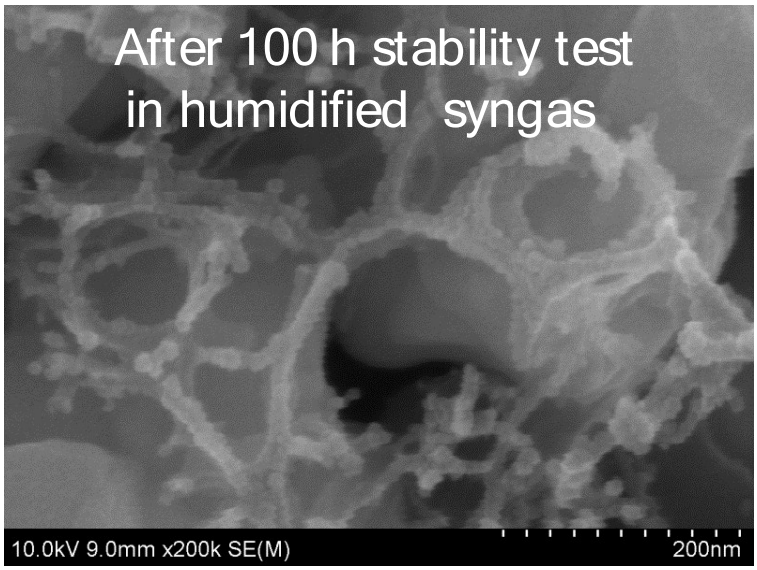

Figure S7 Cross-sectional SEM image of the R-$LS_{0.6}FCN$ cell after 100 h operation at 700 °C under constant voltage of 0.7 V using syngas fuel.

Supplementary References

S1. Z. Feng, E. J. Crumlin, W. T. Hong, D. Lee, E. Mutoro, M. D. Biegalski, H. Zhou, H. Bluhm, H. M. Christen and Y. Shao-Horn, *J. Phys. Chem. Lett.*, 2013, 4, 1512-1518.

S2. C. Yang, Z. Yang, C. Jin, G. Xiao, F. Chen, M. Han, *Adv. Mater.* 2012, *24* (11), 1439-43.

S3. R. Lan, P. I. Cowin, S. S., S. Tao, *Sci. Reports* 2016, *6*, 31839.

S4. J.-h. Myung, D. Neagu, D. N. Miller, J. T. S. Irvine, *Nature* 2016, *537* (7621), 528-531.

S5. Z. Du, H. Zhao, S. Li, Y. Zhang, X. Chang, Q. Xia, N. Chen, L. Gu, K. Świerczek, Y. Li, T. Yang, K. An, *Adv. Energy Mater.* 2018, 1800062.

S6. Z. Yang, Y. Chen, N. Xu, Y. Niu, M. Han, F. Chen, *J. Electrochem. Soc.* 2015, *162* (7), F718-F721.